International Journal of Mechanical Engineering and Technology (IJMET)
Volume 9, Issue 8, August 2018, pp. 220–232, Article ID: IJMET_09_08_024
Available online at http://www.iaeme.com/ijmet/issues.asp?JType=IJMET&VType=9&IType=8
ISSN Print: 0976-6340 and ISSN Online: 0976-6359

APPLICATION OF A MULTI-FUNCTIONAL MEASURING SYSTEM FOR ADAPTIVE EQUALIZATION OF SIGNAL WAVEFORMS AT ULTRASONIC INSPECTION OF PRODUCTS BY NON-CONTACT MOSAIC TRANSDUCERS

V. Kachanov, I. Sokolov, S. Lebedev, M. Karavaev, V. Pervushin and A. Sinitsyn
Moscow Power Engineering Institute, Moscow, Russian Federation

ABSTRACT

It is shown that using the mosaic technology allows for creating ultrasonic low-frequency broadband high-efficiency transducers for non-contact inspection of products made of polymer composite materials by shadow method. It is shown that the lack of mosaic transducers intended to work through the air gap is an uneven amplitude-frequency characteristic easily compensated with multi-functional adaptive measuring system developed by the authors.

Keywords: ultra-sonic low-frequency broadband mosaic transducers, non-contact inspection, frequency-modulated signals, multi-functional adaptive measuring system
Cite this Article: V. Kachanov, I. Sokolov, S. Lebedev, M. Karavaev, V. Pervushin and A. Sinitsyn, Application of a Multi-Functional Measuring System for Adaptive Equalization of Signal Waveforms at Ultrasonic Inspection of Products by Non-Contact Mosaic Transducers, International Journal of Mechanical Engineering and Technology, 9(8), 2018, pp. 220–232.
http://www.iaeme.com/IJMET/issues.asp?JType=IJMET&VType=9&IType=8

1. INTRODUCTION

1.1. Problems of Ultra-Sonic Non-Contact Inspection of Products

Ultrasonic (US) non-destructive inspection (ND) of most products is performed by direct contact of piezoelectric transducers (PET) with the surface of the product under inspection. However, some objects made of polymer composite materials (PCM) allow for neither using immersion liquids nor dry acoustic contact of the transducer with the product surface. In this case, ultra-sonic non-contact PETs working through air gap are used [1–6]. Non-contact ultrasonic inspection has a known disadvantage - low sensitivity due to reflections of ultrasonic vibrations on the media boundary with different acoustic resistances: “PET-air” and “air-PCM”. A whole range of measures are used to increase non-contact inspection sensitivity: - low-frequency signals with an average (resonant) frequency of $f_o \leq 100$ kHz; -

increased sounding signal amplitude (which, however, may be increased only up to a certain limit determined by generator output stage parameters and PET properties); - increased ultrasound radiation efficiency in the air medium and ultrasonic signals receiving efficiency from the air medium by creating special devices for transducer acoustic matching with the air medium. However, all these measures do not fundamentally solve the problem of sensitivity: ultrasonic signal attenuation during passage through the air gap and when reflected from am inspected solid is so great that non-contact inspection is performed mainly in shadow or mirror-shadow mode.

Since ultrasonic non-contact shadow mode allows for using narrow-band quasi-harmonic signals of large amplitude and long duration T_s, then undamped (i.e. highly efficient, but narrow-band) transducers with a relative operating band of $\Delta f/f_o \approx 10\%$ are used in this mode. However, in a number of cases (i.e., with a large dynamic range of recorded signals amplitude changes) and in shadow mode, it is desirable to use short probing signals with a duration of $T_s \approx$ 2-3 periods of carrier frequency [2, 3, 6]. This, in its turn, involves using broadband non-contact PET with a relative transducer bandwidth of $\Delta f/f_o \approx 50\%$.

Thereby, there arises the problem of creating methods for shadow non-contact inspection of products made of PCM, involving simultaneous and broadband transducers and providing high sensitivity of inspection.

2. METHODOLOGY

2.1. Methods for Increasing Sensitivity when Using Non-Contact Transducers

Unfortunately, it is difficult to provide for these two requirements simultaneously, since electroacoustic conversion band broadening is provided, as a rule, due to high-quality piezo transducers damping [2–4] with simultaneous selection of matching layers. Piezo-elements damping, as is known, leads to a loss in efficiency of sensors electroacoustic transformation, and, ultimately, to a decrease in inspection sensitivity [7].

Another way for increasing inspection control through air gap is using high-energy chirp signals (signals with linear carrier frequency modulation) as probing signals, followed by optimal filtering of detected signals [8–11].

Structural diagram of electroacoustic path of ultrasonic shadow non-contact inspection equipment using a chirp signal is shown in Figure 1.

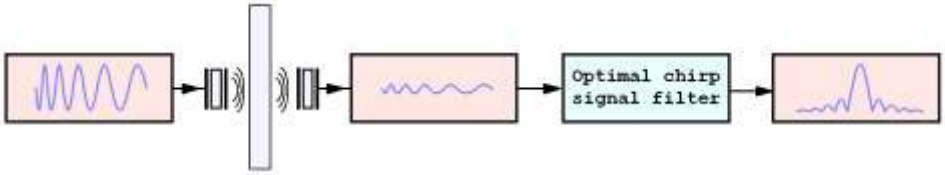

Figure 1 Structural diagram of ultrasonic equipment electroacoustic path of the shadow product inspection through the air gap when using a chirp signal

After passing through the product and through two air gaps, the recorded signal amplitude is greatly attenuated. However, signal-to-noise ratio substantially increases in the receiver path at optimum filter (OF) output for the chirp signal due to its time compression, which compensates for the signal loss at the boundaries of such diverse media.

It should be noted that when inspecting the product shown in Figure 1, the inspection results can be affected by uneven amplitude-frequency response (AFR) of emitting and receiving transducers. In order to exclude this influence, it is necessary to measure transducers AFR before inspection and to compensate for possible chirp signal distortion in sensors.

2.2. Ultrasound Low-Frequency High-Performance Broadband Mosaic Transducers

In this paper we propose using highly sensitive and broadband transducers based on the technology of mosaic composite transducers developed in MPEI in the 1970s [12]. The mosaic transducers technology was originally developed for ultrasonic low-frequency immersion echo-pulse inspection of large-size products made of PCM with large frequency-dependent attenuation. Such mosaic transducers operating in the low-frequency range ($f_o \leq$ 100 kHz) were designed to provide both high sensitivity and wide bandwidth simultaneously, as echo-inspection of products made of PCM required a short, i.e. broadband ultrasound signals with a duration of one to two carrier periods to provide for high resolution: T_s = (1-2)* T_0. This required the development of low-frequency PET with a relative band of $\Delta f/f_o \approx 100\%$. In addition, the conditions for inspecting long products made of PCM required creating low-frequency PETs, which should simultaneously have high electro-acoustic conversion coefficient, as well as relatively high spatial radiation directivity. In order to provide narrow beam:

$$\Theta \approx \arcsin(\lambda/D), \quad (1)$$

where Θ - angle of spatial radiation directivity, D – transducer aperture at the frequency of $f_o \approx 100$ kHz should be not less than 100 mm, λ – wavelength.

However, creating low-frequency monolithic, high-performance broadband PETs with a large aperture causes certain difficulties [12]. First, speaking of monolithic PETs with a large aperture, it is technologically difficult to provide a constant electroacoustic conversion coefficient value over the entire sensor area. Second, when inspecting products with uneven surface, problems arise in ensuring a reliable acoustic contact across the entire transducer area. Third, it is inadvisable to use damping for monolithic transducers with a large aperture.

It was these problems that made us back in the 1970s [12] to replace a monolithic low-frequency transducer with a large aperture of H_2 x H_3 with a composite one, consisting of a set of N identical "elementary" low-frequency piezo-elements with a cross-section of h_2 x h_3, which together formed the same area of H_2 x H_3 (Figure 2).

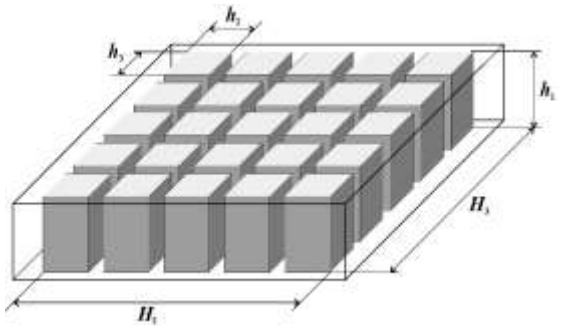

Figure 2 General view of the composite mosaic (matrix, composite) piezoelectric transducer

Identity and repeatability of characteristics of composite PETs with a large aperture was ensured by the selection of PE with same values of height h_1, cross section h_2 x h_3, and electro-acoustic transformation coefficient k_t.

It should be noted that exactly the same composite transducers have become widely used abroad only since 1980 [13, 14] under the name of composite, matrix PETs. This name of composite PETs is explained by the fact that the space between elementary PE is filled with a binder polymer (matrix), whose role is most often played by epoxy resin. As a result, the whole structure becomes similar to a traditional composite material, the characteristics of which (like in any composite material) possess the properties of raw materials. German

scientist H. Splitt believes that composite (matrix, composite) piezoelectric transducers are a "milestone in the development of ultrasonic inspection" [14], since matrix transducers based on piezo-ceramics and epoxy resin, depending on the percentage ratio of piezo-ceramics and polymer, have electro-acoustic transformation coefficient k_t increased; acoustic oscillations speed decreased; acoustic resistance Z decreased; and dielectric constant e_{33} decreased. As a result, composite (matrix) transducers have transmission bandwidth increased by 30-40% without loss in the sensor sensitivity.

However, bandwidth expansion potential of matrix transducers consisting of a one-height PE set is limited. Therefore, then back in the 1970s, MPEI offered the technology of creating low-frequency high-performance broadband composite ultrasonic transducers based on a set of various uneven undamped PEs. We proposed to call similar PETs, composed of various piezoelectric elements as mosaic [12]. Technology of mosaic broadband transducers consisting of uneven piezo-elements set turned out to be especially effective when creating ultra-broadband PETs (Figure 3a).

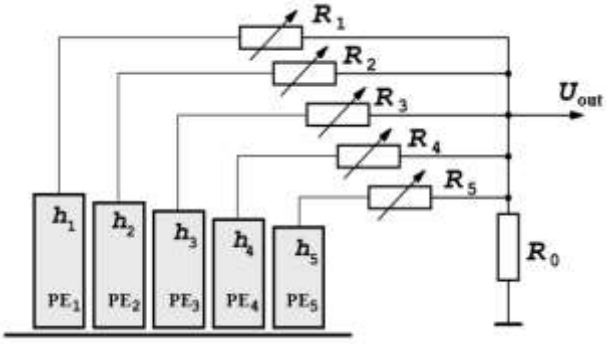

Figure 3 a Principle of designing broadband mosaic PET with a variable AFR form (R_n – balance resistors, U_{out} – output electric signal)

The heights h_n in such transducers were calculated under the following formula:

$$h_n = h_1*[(2Q+1)/(2Q-1)]^{n-1} \quad , \qquad 2$$

where Q is the average value of PE quality factor loaded on the working medium.

Filling in this condition ensures total bandwidth, consisting, as it were, of a "set" of partial AFR of high-quality undamped piezoelectric elements with frequencies f_1, f_2, f_3,.. (Figure 3b).

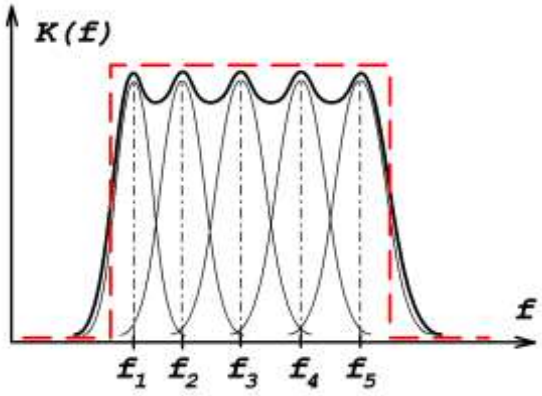

Figure 3 b Broadband mosaic PET AFR with a rectangular shape ($K(f)$ –relative amplitude)

With the help of mosaic technology, it is easy to provide the relative bandwidth of low-frequency PET $\Delta f/f_o \geq 100\%$ without loss in conversion sensitivity (Figure 4).

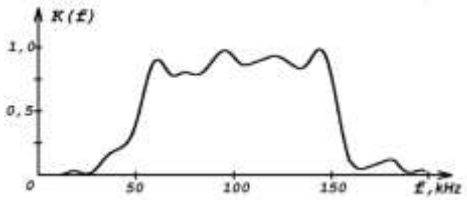

Figure 4 Typical AFR of a broadband mosaic PET

It is possible to create such a band in a low-frequency composite sensor only by selecting optimal combination of piezo-ceramic materials and polymer matrix [15].

The main advantage of composite mosaic transducers from composite ones lies in their constructive variability, which makes it possible to create sensors of any configuration from elementary multi-high PE. In particular, due to the optimization of mosaic elements layout, it was possible to ensure acoustic field even distribution of the low-frequency broadband PETs both in far and in near zone [16].

Thus, mosaic construction technology allowed for producing broadband high-efficiency PETs with frequency and spatial characteristics of a given shape. However, it should be noted that it is possible to achieve an even AFR and even spatial distribution of a mosaic broadband transducer acoustic field using a large number of elementary PEs that differ in small increments Δh in height.

2.3. Application of Broadband Mosaic Transducers for Non-Contact Ultrasonic Inspection

It is obvious that the mosaic technology developed in MPEI for designing low-frequency broadband high-efficiency transducers designed for contact inspecting of products made of PCM was logical to use when creating broadband non-contact PETs. It turned out that it is possible to use the mosaic ideology not only for constructing a broadband high-efficiency PET, but also for creating matching broadband multilayer protectors [5, 6].

During the research, we developed various versions of air-mosaic broadband transducers. Below Figure 5a displays one of them designed to work as part of a shadow inspection device for products made of PCM.

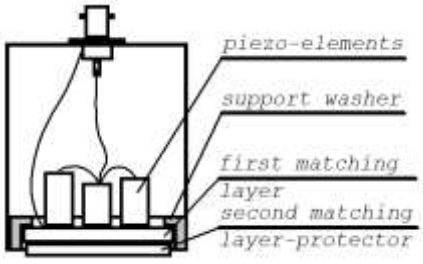

Figure 5 a Non-contact mosaic PET construction sketch

A transducer is a combination of a mosaic PET itself consisting of 9 different piezo-elements with a cross section of 6x6 mm and a multilayer matching composition in the form of several layers connected in series, each of which is made of a polymer material of the original formulation [6]. Unlike contact mosaic transducers, non-contact mosaic PETs have to use a limited number of PE of different heights due to the problem of matching acoustic resistances of piezo-elements of different frequencies with the air medium in a wide frequency band. Therefore, the considered mosaic PET (Figure 5a) has piezo-elements of only

two heights: a transducer consists of four PEs of h = 11 mm in height and five PE of h = 14 mm in height, the topology of which is shown in Figure 5b.

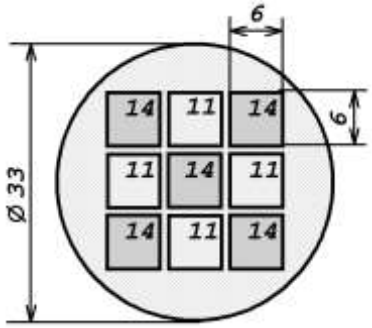

Figure 5 b PE location topology by PET aperture area

The sensor uses two matching layers: The first is made of epoxy resin, the second layer is made of foam plastic. Since PET uses piezoelectric elements of only two heights, the resonant frequencies of the first and second matching layers differ significantly from each other. Therefore, non-contact PETs have a significant unevenness, in contrast to mosaic PETs for contact inspection, consisting of a large number of PEs.

2.4. Compensation of Ultrasonic Signals Distortions in Non-Contact Transducers due to Adaptive Correction of Their Amplitude-Frequency Spectrum

AFR unevenness of a non-contact PET leads to combined AFR unevenness of the entire electroacoustic path, shown in Figure 1, in which the mosaic transducers participate as the radiating and receiving ultrasonic low-frequency transducers. As a result, due to AFR unevenness of each sensor, the compressed pulse shape is distorted after optimal filter and, thereby, the reliability of the control is reduced.

In the early stages of creating mosaic broadband transducers, sensor AFR unevenness was equalized by means of weight resistors, as shown in Figure 3a. However, with this method of correcting AFR unevenness, electroacoustic conversion coefficient value of the broadband sensor is markedly reduced. For more effective amplitude-frequency correction, we created an automatic algorithm for compensating distortions with the help of software and hardware multi-functional adaptive measuring system (MS) [17], which made it possible to significantly improve the shape of the signal distorted in non-contact PETs, making it more even and close to the sounding signal form. The distortion compensation was performed with the help of an installation (Figure 6), consisting of a radiating and receiving mosaic PETs, as well as a measuring system consisting of a personal computer such as an IBM PC containing DAC/ADC boards.

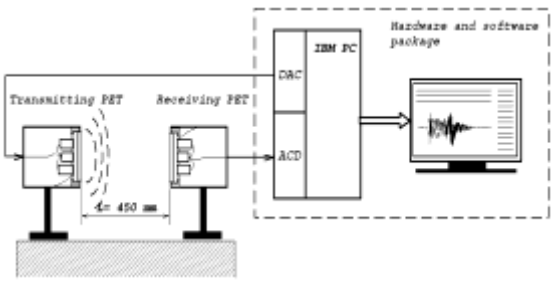

Figure 6 Experimental installation diagram of efficiency study of the algorithm for adaptive correcting the registered echo-signals forms

A chirp signal (Figure 7a) was used in the experiment, the spectrum of which has a rectangular envelope curve (b). At OF output, undistorted chirp signal has the form of a compressed signal (c); chirp signal after OF and the synchronous demodulator (SD) is shown in Figure 7d [18].

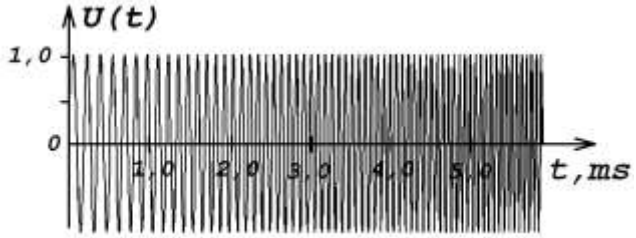

Figure 7 a Sounding chirp signal *U(t)*

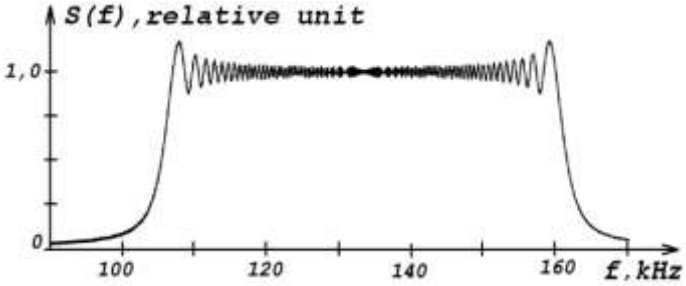

Figure 7 b Amplitude spectrum *S(f)* of chirp signal

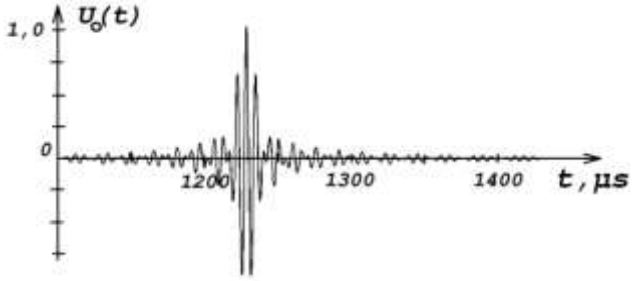

Figure 7 c Chirp signal form at optimal filter output $U_o(t)$

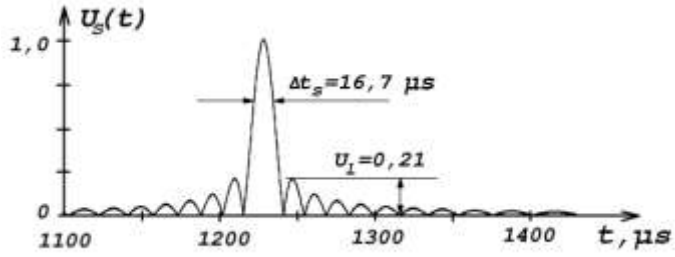

Figure 7 d Compressed chirp signal form $U_s(t)$ after synchronous demodulator

Distorted chirp signal (Figure 8a) differs significantly from the sounding signal (Figure 7a).

Figure 8 a Chirp signal $U_d(t)$ distorted in electroacoustic path

In the process of distortion compensation, the distorted signal spectrum $S_d(f)$ that passed through the frequency-dependent path (Figure 8b) was compared with the emitted signal spectrum $S(f)$ (Figure 7b).

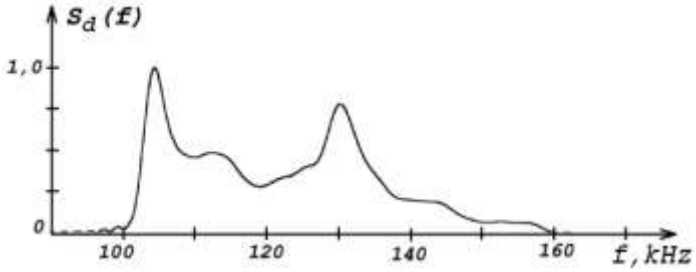

Figure 8 b Chirp signal $U_d(t)$ amplitude frequency spectrum $S_d(f)$

Then, the distortion level was evaluated and as a result, the amplitude-frequency weight function $W(f)$ was formed (Figure 9), which was calculated as a quotient of values division of chirp signals spectra $S(f)$ and $S_d(f)$.

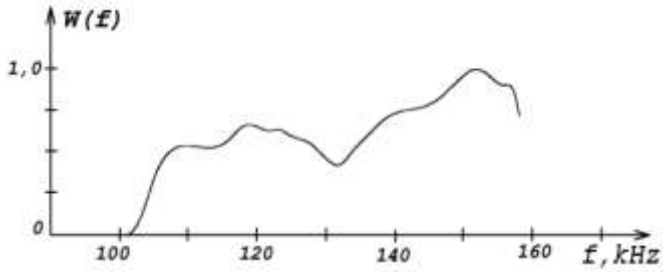

Figure 9 Weight function $S_w(f)$, intended to compensate for distortions in the amplitude spectrum of the distorted chirp signal

The received weight function $W(f)$ allows for compensating amplitude-frequency distortions of chirp signal in this path by multiplying function $W(f)$ by the received signals spectrum.

3. RESULTS

3.1. Chirp Signal Spectrum Distortion Compensation Results in Mosaic Non-Contact Broadband High-Sensitivity Transducers

Figures 10-12 display an example of compensating distorted chirp signal in an electroacoustic path consisting of radiating and receiving non-contact PETs located opposite each other (Figure 6).

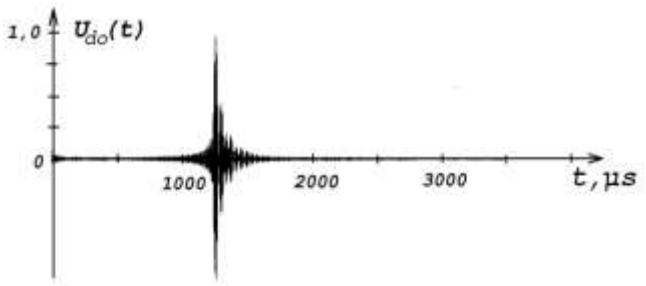

Figure 10 a "Compressed" chirp signal $U_{do}(t)$ in OF

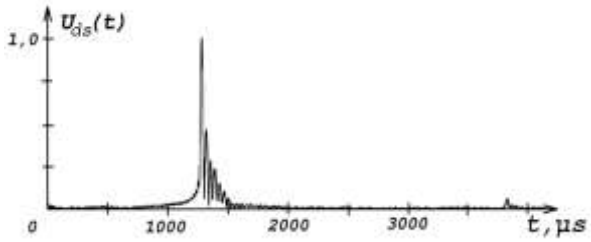

Figure 10 b Distorted chirp signal after synchronous detection $U_{ds}(t)$

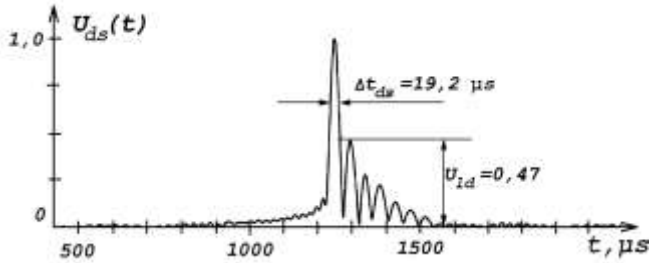

Figure 10 c Fragment of the distorted chirp signal $U_{ds}(t)$ on an enlarged scale

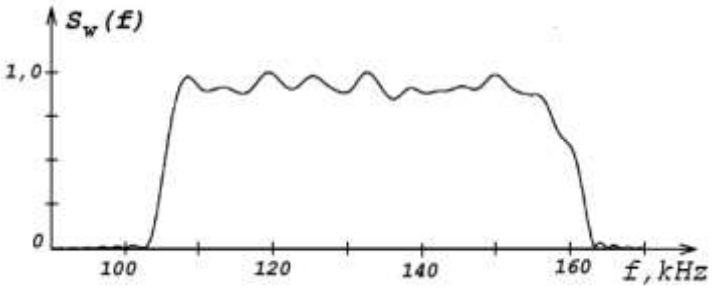

Figure 11 Compensated spectrum $S_w(f)$ of the received chirp signal

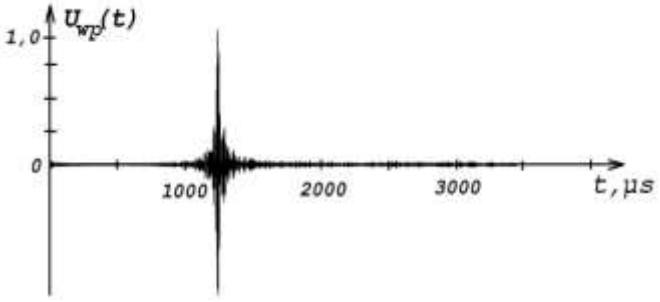

Figure 12 a Diagram of the signal recovered as a result of the weight processing chirp signal at OF output

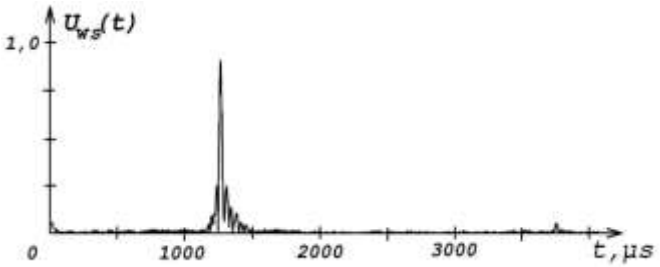

Figure 12 b "Compressed" chirp signal diagram after synchronous detection

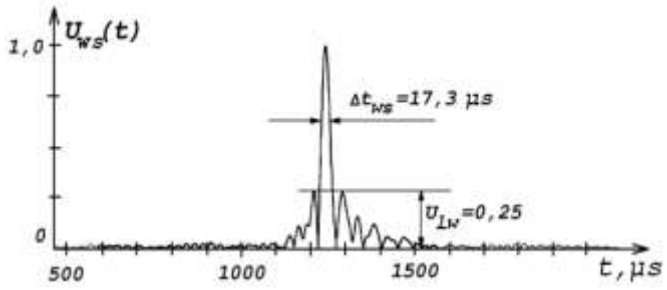

Figure 12 c Signal fragment diagram at synchronous demodulator output on an enlarged scale

The signal received by the receiving transducer spectrum $S_d(f)$ (Figure 8b) has two characteristic peaks that correspond to high-quality PEs resonances of h = 11 mm and h = 14 mm and low-good matching layers resonances. Obviously, the width and shape of the spectrum in Figure 8b does not correspond to initial sounding chirp signal spectrum (Figure 7b). This distortion also affects the form of the "squeezed" in time chirp signal at OF output (Figure 10). In more detail, "compressed" chirp signal distortion appears after synchronous detection (Figure 10b), as well as on its fragment, shown on an enlarged scale in Figure 10c.

Since probing chirp signal frequency deviation is $\Delta f_{cs} \approx 60$ kHz, the expected duration t_s of the signal at optimal filter output should be of the order of t_s = 16.7 μs. Due to spectrum distortion of $S_d(f)$, "compressed" distorted signal duration t_{ds} is increased and is of the order of t_{ds} = 19.2 microseconds, which is 15% higher than the calculated value of t_s. "Compressed" signal shape is not symmetrical, and the relative amplitude level of the maximum side lobe is U_{ld} = 0.47, which exceeds the theoretical level by almost 2.5 times. A significant level of side lobes significantly reduces inspection results reliability, as it masks closely located pulses of smaller amplitude.

In the measuring complex developed by us, when using the "Automatic AFR correction" operating mode, the weight function $W(f)$ (Figure 9) and the received distorted signal frequency spectrum $S_d(f)$ are multiplied (Figure 8b). As a result, compensated spectrum form is reduced to practically classical form of chirp signal spectrum (Figure 11).

4. DISCUSSION

The diagrams of the corrected (reduced) "compressed" chirp signal are shown in Figure 12a. Figure 12b shows a chirp signal after optimum filter and synchronous demodulator, and Figure 12 displays its fragment on an enlarged scale.

After weight correction, spectrum shape of $S_w(f)$ of the detected signal was restored almost completely (Figure 11), and compressed signal duration Δt_{ws} in comparison with t_{ds} duration was reduced to Δt_{ws} = 17.3 μs (Figure 12c), what is only 3% more than the calculated value of Δt_s. Compressed signal shape has acquired a practically symmetrical form, and the

relative level of the maximum side lobe is equal to U_{lw} = 0.25, which exceeds the theoretical level by only 15%.

Another indicator of signal distortions qualitative compensation is the fact that when the distance between the radiating and receiving transducers in the range from 100 to 1000 mm was changed (see the experimental setup diagram in Figure 1), only a proportional increase in the recorded signal delay occurred and practically did not change it form, which made it possible to use the weight function obtained for a given electroacoustic path without any adjustment.

Thus, chirp signal distortion correction in mosaic broadband high-sensitivity non-contact transducers allows for being used later for monitoring products made of PCM according to the diagram shown in Figure 1, in order to establish the frequency characteristics of the inspected product without affecting the inspection result of broadband mosaic non-contact PETs characteristics.

5. CONCLUSION

The research results show that using the mosaic construction technology makes it possible to create a broadband high-efficiency low-frequency piezoelectric transducer for operation in non-contact ultrasonic inspection equipment. Mosaic construction principles also make it possible to provide effective broadband acoustic matching of such diverse materials as piezo-ceramics and air. A drawback, inevitably inherent in discrete constructions of mosaic converters - the amplitude-frequency characteristic unevenness, which is manifested in practice in distortions of recorded signals form - can be largely eliminated using adaptive amplitude-frequency weighing of registered ultrasonic signals.

The result of electroacoustic path correction is the possibility of measuring frequency characteristics of the inspected products from polymer composite materials without fear of possible inspection results distortion due to the influence of the non-contact transducers characteristics on them.

ACKNOWLEDGEMENTS

The article is prepared within the framework of the State Task no. 9.7168.2017/6.7 to educational organizations of higher education, subordinated to the Ministry of Education and Science of Russia, in the field of scientific activity for the work “Organization of scientific research”.

REFERENCES

[1] Shkarlet, Yu. M. Non-Contact Methods of Ultrasonic Testing. Moscow: Machine Building, 1974, pp. 56.

[2] Bhardwaj, M. C. Non-Destructive Evaluation: Introduction of Non-Contact Ultrasound. In: Schwartz, M., ed., Encyclopedia of Smart Materials. New York: John Wiley & Sons, 2002 pp. 690-714.

[3] Bhardwaj, M. C. Evolution of Piezoelectric Transducers to Full Scale Non-Contact Ultrasonic Analysis Mode. Proceedings World Conference on Non-Destructive Testing, Montreal, 2004.

[4] Hillger, W., Meier, R. and Henrich, R. Inspection of CFRP Components by Ultrasonic Imaging with Air-Coupling. Insight - Non-Destructive Testing and Condition Monitoring, 46(3), 2004, pp. 147-150. http://www.ingentaconnect.com/contentone/bindt/insight/2004/00000046/00000003/art00005

[5] Aksenov, V. P. and Volosskii, V. P. Ultrasonic Transducer for Operation in the Air. USSR Authorship Certificate SU 1167494 Bulletin No. 26, 1985.

[6] Kachanov, V. K., Sokolov, I. V. and Karavaev, M. A. Development of an Ultraacoustic Mosaic Wideband Piezoelectric Transducer for Contactless Testing of Articles Made of Polymer Composite Materials. Measurement Techniques, 58(2), 2015, pp. 203-207. https://link.springer.com/article/10.1007/s11018-015-0686-2

[7] Yermolov, I. N. Ultrasonic Transducers for Non-Destructive Testing. Moscow: Machine Building, 1986.

[8] Gan, T. H., Hutchins, D. A., Billson, D. R. and Schindel, D. W. The Use of Broadband Acoustic Transducers and Pulse-Compression Techniques for Air-Coupled Ultrasonic Imaging. Ultrasonics, 39(3), 2001, pp. 181-194. https://www.sciencedirect.com/science/article/pii/S0041624X00000597

[9] Pallav, P., Gan, T. H. and Hutchins, D. A. Elliptical-Tukey Chirp Signal for High-Resolution, Air Coupled Ultrasonic Imaging. IEEE Transactions on Ultrasonics Ferroelectrics and Frequency Control, 54(8), 2007, pp. 1530-1540. https://ieeexplore.ieee.org/document/4291502/

[10] Ricci, M., Senni, L. and Burrascano, P. Exploiting Pseudorandom Sequences to Enhance Noise Immunity for Air-Coupled Ultrasonic Nondestructive Testing. IEEE Transactions on Instrumentation and Measurement, 61(11), 2012, pp. 2905-2915. https://ieeexplore.ieee.org/document/6222332/

[11] Hutchins, D., Burrascano, P., Davis, L., Laureti, S. and Ricci, M. Coded Waveforms for Optimized Air-Coupled Ultrasonic Nondestructive Evaluation. Ultrasonics, 54(7), 2014, pp. 1745-1759. https://www.sciencedirect.com/science/article/pii/S0041624X14000626

[12] Aksenov, V. P., Popov, I. S., Popko, V. P., Kachanov, V. K. and Pitolin, A. I. Application of Piezo-Ceramic Mosaic Electroacoustic Transducers. MPEI Works, 335, 1975, pp. 49-52.

[13] Newnham, R. E. Composite Piezoelectric Transducers. Mater. Eng, 2, 1980, pp. 93-106.

[14] Splitt, G. Piezocomposite Transducers - a Milestone for Ultrasonic Testing. Insight - Non-Destructive Testing and Condition Monitoring, 40(11), 1998, pp. 760-763.

[15] Kachanov, V. K., Sokolov, I. V., Konov, M. M. and Sinitsyn, A. A. Comparison of the Features of Composite and Mosaic Piezotransducers for the Ultrasonic Testing of Products with a High Attenuation Level of Ultrasonic Signals. Russian Journal of Nondestructive Testing, 47(8), 2011, pp. 532-544. https://link.springer.com/article/10.1134/S1061830911080067

[16] Kachanov, V. K., Sokolov, I. V., Konov, M. M., Timofeev, D. V. and Sinitsyn, A. A. Spatiotemporal Characteristics of Broadband Ultrasonic Transducers. Russian Journal of Nondestructive Testing, 46(10), 2010, pp. 718-728. https://link.springer.com/article/10.1134/S1061830910100025

[17] Kachanov, V. K., Sokolov, I. V., Kontsov, R. V., Sinitsyn, A. A. and Fedorov, M. M. Adaptive Instruments for Ultrasonic Nondestructive Testing of Large Objects with Complex Structures. Russian Journal of Nondestructive Testing, 52(5), 2016, pp. 251-260. https://link.springer.com/article/10.1134/S106183091605003X

[18] Kachanov, V. K. and Sokolov, I. V. Application Features of Radio Engineering Signal Processing Methods for Ultrasonic Flow Detection. Nondestr. Test. Eval., 15, 2000, pp. 330-360.

LIST OF CHARACTERS

h_i – size of the piezoelectric element [mm]
H_i – size of the piezoelectric transducer [mm]
f – frequency [kHz]
f_o – average (resonant) frequency (piezoelectric element/ transducer) [kHz]
$\Delta f/f_o$ – transducer bandwidth [relative unit]
T_s – duration of probing signals [μs]
T_0 – duration of carrier period [μs]
D – transducer aperture [mm]
λ – wavelength [m]
Θ – angle of spatial radiation directivity [˚]
k_t – electro-acoustic transformation coefficient [V/mm]
Z – acoustic resistance [ohm]
e_{33} – dielectric constant [relative unit]
Q – average value of PE quality factor [relative unit]
R_n – balance resistors [ohm]
U_{out} – output electric signal [V/mm]
$K(f)$ –relative amplitude [relative unit]
$S_i(f)$ – amplitude spectrum [relative unit]
Δt_i – times increments [μs]
Δt_{ws} – [μs]
Δt_s – [μs]
U_{lw} – [V]
U_{ds} – [V]
U_d – [V]
U_0 – [V]
U_s – [V]
U_{ws} – [V]
Δh – heights increments [mm]
$U_i(t)$ – time dependence of the signal voltage[V]
$W(f)$ – weight function [relative unit]
Δf_{cs} –frequency deviation of the chirp signal